

Study on Structural and Dielectric Behavior of $\text{Li}_{0.3}\text{Zn}_{0.3}\text{Co}_{0.1}\text{Fe}_{2.3}\text{O}_4$

Madhumita Dalal^{1,2*}, Sukhendu Sadhukhan² and Pabitra K. Chakrabarti²

¹Department of Physics, Bejoy Narayan Mahavidyalaya, Hooghly, West Bengal, India

²Department of Physics, Burdwan University, Burdwan, West Bengal, India

*Correspondence to:

Madhumita Dalal
Department of Physics,
Bejoy Narayan Mahavidyalaya,
Hooghly, West Bengal, India.

Department of Physics,
Burdwan University,
Burdwan, West Bengal, India.

E-mail: dalal.madhumita@gmail.com

Received: January 03, 2024

Accepted: March 15, 2024

Published: March 20, 2024

Citation: Dalal M, Sadhukhan S, Chakrabarti PK. 2024. Study on Structural and Dielectric Behavior of $\text{Li}_{0.3}\text{Zn}_{0.3}\text{Co}_{0.1}\text{Fe}_{2.3}\text{O}_4$. *NanoWorld J* 10(S1): S246-S249.

Copyright: © 2024 Dalal et al. This is an Open Access article distributed under the terms of the Creative Commons Attribution 4.0 International License (CCBY) (<http://creativecommons.org/licenses/by/4.0/>) which permits commercial use, including reproduction, adaptation, and distribution of the article provided the original author and source are credited.

Published by United Scientific Group

Abstract

Nanoparticles of $\text{Li}_{0.3}\text{Zn}_{0.3}\text{Co}_{0.1}\text{Fe}_{2.3}\text{O}_4$ are prepared by sol-gel method using nitrate salts as precursor materials. Two different sizes (16.9 and 38.9 nm) are obtained by annealing the sample at 500 and 600 °C, respectively. X-ray diffraction (XRD) patterns of the two samples exhibit only the desired peaks of cubic $\text{Fd}\bar{3}\text{m}$ space group which confirms the pure spinel ferrite phase formation in the samples. Size and root mean square (r.m.s.) lattice strains are obtained by Williamson-Hall method. The r.m.s. lattice strains of the two samples are 1.25×10^{-4} and 1.15×10^{-3} , respectively which confirms that the prepared samples are free from appreciable defects. The dielectric constants of the two samples are studied as functions of temperature and frequency. Dielectric behavior of the samples is explained by the electronic exchange between ferrous and ferric ions. Thermal variation of the dielectric constant shows that there is a phase transition from ferroelectric to paraelectric phase for both the samples at ~ 320 K. Dielectric constant decreases with the increase of frequency which is since beyond a certain frequency of the externally applied electric field, the electronic exchange between the Fe^{2+} and Fe^{3+} ions fail to follow the applied electric field.

Keywords

Ferrite, Sol-gel method, X-ray diffraction, Williamson-Hall method, Dielectric constant

Introduction

Polycrystalline spinel ferrites are widely known for their important structural, magnetic, and dielectric behaviors and interestingly, these properties could be tuned by proper choice of metal cations and by varying the average crystallite size ($\langle d_{\text{cryst}} \rangle$). Spinel ferrites have formula unit described by AOB_2O_3 where A- and B- are two lattice voids surrounded by four and six oxygen anions, respectively. Metal cations occupy these voids and depending on the metal cations structural, magnetic, and dielectric behaviors change.

Frequency dependence of dielectric constant of lithium ferrite is studied by Teixeira et al. [1] and the dielectric behavior of substituted lithium ferrites is studied by many researchers which include nickel [2], cobalt [3, 4], cadmium [5], manganese [6] substituted lithium ferrites. Earlier studies indicate that the substituting metals significantly affect the dielectric behavior of the lithium ferrite. In this paper, the frequency dependence and temperature dependence of lithium-zinc-cobalt ferrite is included.

Experimentation

Sample preparation

Polycrystalline ferrite samples of general formula $\text{Li}_{0.3}\text{Zn}_{0.3}\text{Co}_{0.1}\text{Fe}_{2.3}\text{O}_4$ are prepared by sol-gel method where LiNO_3 , $\text{Zn}(\text{NO}_3)_2 \cdot 6\text{H}_2\text{O}$, $\text{Co}(\text{NO}_3)_2 \cdot 6\text{H}_2\text{O}$ and $\text{Fe}(\text{NO}_3)_3 \cdot 9\text{H}_2\text{O}$ are used as precursor materials. Nitrate salts are taken in the chosen stoichiometric ratio and dissolved in deionized water by employing a magnetic stirrer. Aqueous solution of equimolar citric acid is added to the aqueous nitrate solution while stirring is maintained. Stirring is continued further until a gel is formed and on gel formation the beaker is shifted to an oven to burn the excess nitrates. The product is then powdered and annealed at two different temperatures (500 and 600 °C) and the samples are named as LZC5 and LZC6, respectively.

Characterizations

XRD patterns of LZC5 and LZC6 samples are recorded in powder X-ray diffractometer, Model BRUKER D8 Advance with da Vinci, using $\text{CuK}\alpha$ radiation ($\lambda=1.5405\text{\AA}$). Dielectric measurements of LZC5 and LZC6 samples are recorded by HIOKI 3532-50 LCR HiTESTER over the frequency range of 100 Hz to 5 MHz at different temperatures (300 to 450 K). For dielectric measurement, LZC5 and LZC6 powder samples are pressed into the cylindrical shaped pellets (thickness ~ 0.05 cm and diameter ~ 0.8 cm) using hydraulic press and electrodes are formed on the two flat faces of these pellets using silver coating.

Results and Discussion

XRD study

XRD patterns of the samples LZC5 and LZC6 are displayed in figure 1. Diffraction peaks corresponding to the cubic $\text{Fd}\bar{3}\text{m}$ space group only are appeared in the XRD patterns of both the samples which confirm pure phase formation in the prepared samples. Williamson-Hall method is employed to derive $\langle d_{\text{cryst}} \rangle$ and r.m.s. lattice strain. For this purpose, obtained XRD patterns are fitted with multiple (six) peaks of Gauss type and the $\beta \cos\theta$ vs $4\sin\theta$ graphs are plotted with the β (full width at half maximum) and θ (peak angle) derived from multiple peaks fitting. Linear fitting is performed on these Williamson-Hall plots ($\beta \cos\theta$ vs $4\sin\theta$) and $\langle d_{\text{cryst}} \rangle$ and r.m.s. lattice strains are calculated from the slope and intercept of the fitted straight line. The obtained values of $\langle d_{\text{cryst}} \rangle$ and r.m.s. lattice strain of LZC5 and LZC6 samples are 16.9, 38.9 nm and 1.25×10^{-4} , 1.15×10^{-3} , respectively which agree with those derived using Rietveld method [7].

Dielectric properties

Variation of dielectric constant with frequency

Dielectric polarization in ferrites occurs through the exchange of electrons between Fe^{2+} and Fe^{3+} ions. Electron exchanges between the $\text{Fe}^{2+} \leftrightarrow \text{Fe}^{3+}$ results in local displacement of charges which is responsible for polarization in ferrites [3]. In polycrystalline ferrites, the grain boundaries restrict this local displacement of charges and results in high resistivity. Variation of dielectric constant (ϵ') of LZC5 and LZC6 samples as

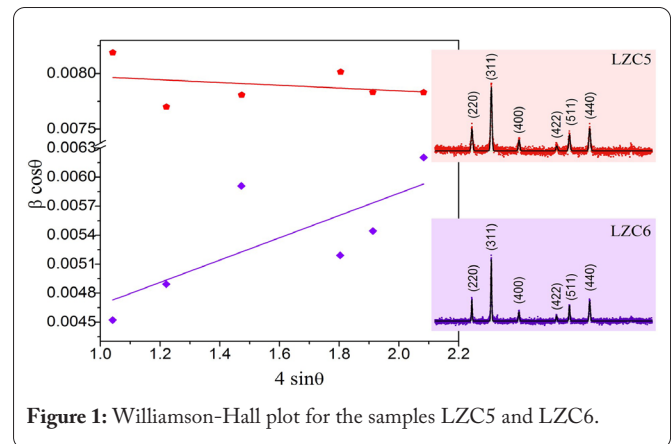


Figure 1: Williamson-Hall plot for the samples LZC5 and LZC6.

a function of frequency at different temperatures is displayed in figure 2. Dielectric constant of both the samples decreases with increase of frequency which indicates towards the presence of relaxation in both the samples. But the relaxation deviates from the ideal nature of Debye relaxation and can be explained by Cole-Cole relaxation. According to Cole-Cole relaxation, the dielectric constant is described by equation 1.

$$\epsilon'(\omega) = \epsilon_{\infty} + \frac{\Delta\epsilon \left\{ 1 + (\omega\tau)^{1-\alpha} \sin\left(\frac{\alpha\pi}{2}\right) \right\}}{1 + 2(\omega\tau)^{1-\alpha} \sin\left(\frac{\alpha\pi}{2}\right) + (\omega\tau)^{2(1-\alpha)}} \quad (1)$$

Where ω is the angular frequency, $\Delta\epsilon = \epsilon_0 - \epsilon_{\infty}$ is the dielectric relaxation strength, ϵ_0 and ϵ_{∞} are low frequency and high frequency permittivity limits, respectively, τ is the relaxation time corresponding to the maximum loss and α is the shape parameter [8]. $\alpha = 0$ gives the Debye form of relaxation while non-zero values of α denotes the deviation from Debye form.

In the low frequency region, ϵ' increases rapidly with the decrease of frequency and has very high value ~ 3000 . The variation of ϵ' in the low frequency region is dominated by the interfacial polarization effect, which follows the Koop's phenomenological theory and known as the Maxwell-Wagner polarization [4]. Nanoparticles consist of conductive grains bounded by resistive walls which cause to develop polarization at the interface of grain boundaries. At low frequency, this polarization follows the electric field but at high frequencies the polarization can't follow the electric field and causes a sharp drop in the value of ϵ' . Thus, to avoid the interfacial polarization, the data recorded above the frequency of $\sim 10^3$ Hz is considered while fitting by Cole-Cole equation (Equa-

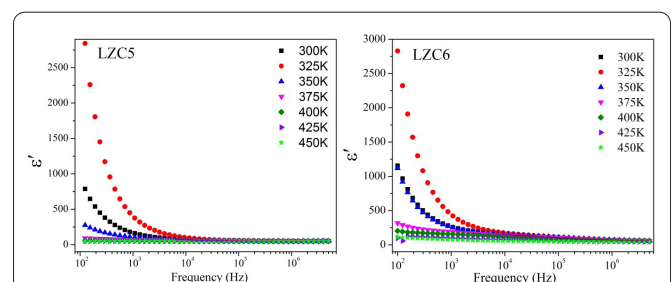


Figure 2: Frequency variation of dielectric constant.

Table 1: Results of Cole-Cole fitting.

Sample	T (K)	ϵ_0	ϵ_∞	$\Delta\epsilon = \epsilon_0 - \epsilon_\infty$	$\tau \times 10^5 \text{ s}$	α
LZC5	300	165	49	116	8.28	0.34
	325	320	49	271	6.75	0.26
	350	94	48	46	3.00	0.35
	375	63	48	15	1.63	0.33
LZC6	300	236	43	193	0.96	0.56
	325	637	31	606	53.4	0.67
	350	232	34	198	0.56	0.64
	375	211	20	191	0.36	0.70

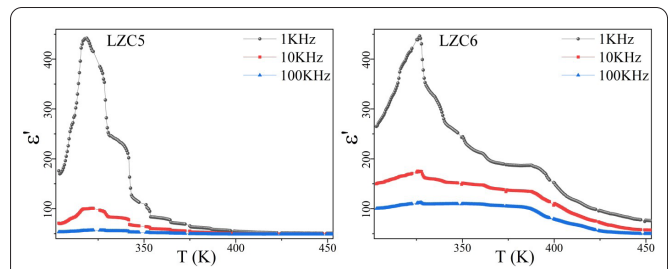
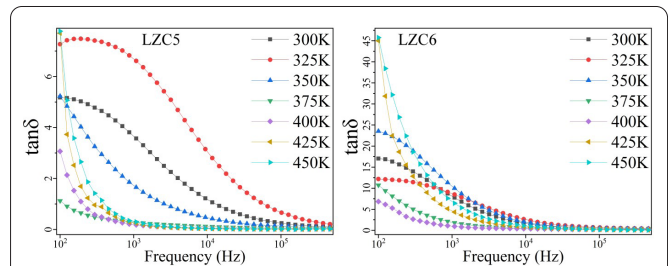
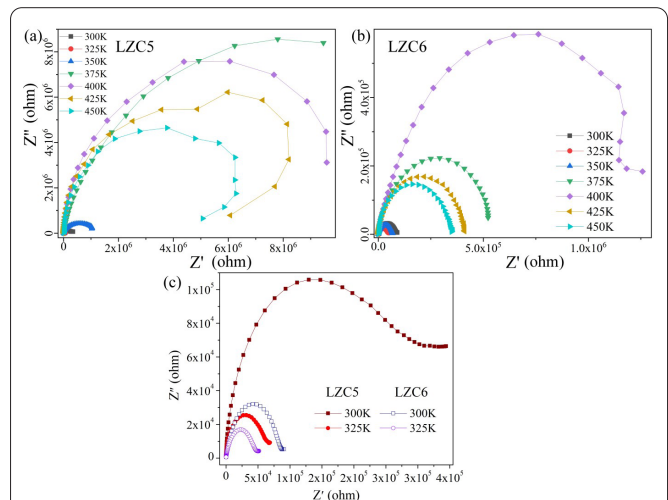
tion 1) and fitted parameters are listed in table 1. The dielectric strength ($\Delta\epsilon$) of LZC6 is higher than that of LZC5 which is because LZC6 having larger $\langle d_{\text{cryst}} \rangle$ (= 38.9 nm) compared to LZC5 (16.9 nm) and therefore has larger grain boundaries, i.e. more interfacial polarizations. The shape parameter ranges from 0.26 - 0.70 in the temperature range 300 - 375 K. Above 375 K, ϵ' becomes very small, so Cole-Cole fitting is avoided above 375 K. High frequency permittivity and relaxation time is relatively higher in LZC5 than LZC6.

Variation of dielectric constant with temperature

Temperature variation of ϵ' of LZC5 and LZC6 samples recorded at frequencies 1, 10 and 100 kHz is shown in figure 3. At 10 and 100 kHz frequencies, ϵ' remains independent of temperature but at a frequency of 1 kHz, ϵ' increases up to a certain temperature and then decreases abruptly with further increase of temperature. Thus, a transition from ferroelectric to paraelectric phase occurs at this temperature (T_c). The value of T_c for LZC5 and LZC6 samples are 319 and 327 K, respectively. Such temperature variation of ϵ' can also be explained by the presence of grain boundaries in polycrystalline ferrites. At higher temperatures grain boundaries start to disappear, thereby causing a drop in interfacial polarization which in turn results in a drop of ϵ' . Larger $\langle d_{\text{cryst}} \rangle$ of LZC6 causes a larger T_c in this sample.

Variation of loss tangent with frequency

Effect of frequency on the loss tangent ($\tan\delta$) of LZC5 and LZC6 samples at different temperatures is shown in figure 4. The sample, LZC5 has very small value of $\tan\delta$ compared to LZC6 sample, however in both the samples $\tan\delta$ decreases with the increase of frequency. $\tan\delta$ represent the energy loss per cycle which comes from two components, one from the polarization part and other from the leakage part. As discussed earlier, the interfacial polarization decreases at high frequencies, thus $\tan\delta$ decreases at high frequencies. The loss curves at temperatures 300 - 350 K are different from those at other temperatures. None of the curves exhibit a loss peak except for that of LZC5 sample at 325 K. Generally, a loss peak i.e. the maximum value of $\tan\delta$ occurs at a frequency when the hopping frequency becomes equal to frequency of the applied field. At temperatures above 350 K, $\tan\delta$ drops abruptly at higher frequency which is due to the disappearance of Maxwell-Wagner polarization above this temperature.

**Figure 3:** Temperature variation of dielectric constant.**Figure 4:** Frequency variation of dielectric loss tangent.**Figure 5:** $Z' - Z''$ plot at different temperatures.

Variation of complex impedances at different temperatures

$Z' - Z''$ plot of LZC5 and LZC6 samples are shown in figure 5. The plots display some depressed semi-circles with their centres below the real axis, thereby suggesting a non-Debye type relaxation. It is clear from the plots that both the samples have high grain boundary resistance which is a primary requirement for good dielectrics. Additionally, the slope of $Z' - Z''$ plot of the sample LZC6 is greater than that of LZC5 sample which could be attributed to the drastic change in nanoparticles sizes including the non-uniformity of grain boundaries of the former.

Conclusion

Polycrystalline nanoparticles of $\text{Li}_{0.3}\text{Zn}_{0.3}\text{Co}_{0.1}\text{Fe}_{2.3}\text{O}_4$ are prepared by sol-gel method and their structural and dielectric properties are studied. Nano-crystallites of sizes 16.9 and 38.9 nm show very small values of r.m.s. lattice strains 1.25

$\times 10^{-4}$ and 1.15×10^{-3} , respectively which confirm minimized crystal defects in the prepared samples. Dielectric constant of both the samples decreases at higher frequency and high dielectric constant at lower frequency is due to the Maxwell-Wagner type interfacial polarization. At higher temperatures, this polarization decreases abruptly, and loss tangents take a constant value at high temperatures as well as high frequencies. The dielectric strength of LZC6 sample (38.9 nm) at 325 K is maximum (606), so the break down voltage for this sample will be maximum. Hence, nanoparticles of $\text{Li}_{0.3}\text{Zn}_{0.3}\text{Co}_{0.1}\text{Fe}_{2.3}\text{O}_4$ with $\langle d_{\text{cryst}} \rangle$ of 38.9 nm could be considered as a potential dielectric candidate when dielectric strength will be main concern. But when overall performance is a concern, then considering higher value of impedance, high frequency permittivity, and relaxation time along with lower dielectric loss LZC5 will be a potential dielectric for application cases.

Acknowledgments

Authors want to acknowledge WBDST (292(Sanc.)/ST/P/S&T/16G-28/2017, Dated: 28.03.2018) for their financial support of this work. Authors wish to acknowledge DST-SERB, Govt. of India (EMR/2017/000832, Dated: 19.03.2018) for the financial assistance. Authors also want to acknowledge the financial support provided by UGC, Govt. of India, through the CAS program (No. F.530/20/CAS-II/2018 (SAP-I), Dated: 25.07.2018), FIST, DST Govt. of India (Ref: SR/FST/PS-II/2018/52, TPN No- 19862,) and PURSE-II, DST, Govt. of India (No. SR/PURSE Phase-2/34, Dated: 27.02.2017).

Conflict of Interest

The authors declare that they have no known competing financial interests or personal relationships that could have appeared to influence the work reported in this paper.

References

1. Teixeira SS, Graça MP, Costa LC. 2012. Dielectric, morphological, and structural properties of lithium ferrite powders prepared by solid state method. *J Non Cryst Solids* 358(16): 1924-1929. <https://doi.org/10.1016/j.jnoncrsol.2012.06.003>
2. Reddy PV, Reddy VD. 1994. Far-infrared spectral studies of some lithium-nickel mixed ferrites. *J Magn Magn Mater* 136(3): 279-283. [https://doi.org/10.1016/0304-8853\(94\)00321-1](https://doi.org/10.1016/0304-8853(94)00321-1)
3. Venudhar YC, Mohan KS. 2002. Dielectric behaviour of lithium-cobalt mixed ferrites. *Mater Lett* 54(2-3): 135-139. [https://doi.org/10.1016/S0167-577X\(01\)00551-1](https://doi.org/10.1016/S0167-577X(01)00551-1)
4. Watawe SC, Sarwade BD, Bellad SS, Sutar BD, Chougule BK. 2000. Microstructure, frequency and temperature-dependent dielectric properties of cobalt-substituted lithium ferrites. *J Magn Magn Mater* 214(1-2): 55-60. [https://doi.org/10.1016/S0304-8853\(00\)00033-0](https://doi.org/10.1016/S0304-8853(00)00033-0)
5. Watawe SC, Bamne UA, Gonbare SP, Tangsali RB. 2007. Preparation and dielectric properties of cadmium substituted lithium ferrite using microwave-induced combustion. *Mater Chem Phys* 103(2-3): 323-328. <https://doi.org/10.1016/j.matchemphys.2007.02.037>
6. Hankare PP, Patil RP, Sankpal UB, Jadhav SD, Mulla IS, et al. 2009. Magnetic and dielectric properties of nanophase manganese-substituted lithium ferrite. *J Magn Magn Mater* 321(19): 3270-3273. <https://doi.org/10.1016/j.jmmm.2009.05.074>
7. Dalal M, Greneche JM, Satpati B, Ghzaïel TB, Mazaleyrat F, et al. 2017. Microwave absorption and the magnetic hyperthermia applications of $\text{Li}_{0.3}\text{Zn}_{0.3}\text{Co}_{0.1}\text{Fe}_{2.3}\text{O}_4$ nanoparticles in multiwalled carbon nanotube matrix. *ACS Appl Mater Interfaces* 9(46): 40831-40845. <https://doi.org/10.1021/acsami.7b12091>
8. Dey CC, Sadhukhan S, Mitra A, Dalal M, Shaw A, et al. 2021. Magnetic energy morphing, capacitive concept for $\text{Ni}_{0.3}\text{Zn}_{0.4}\text{Ca}_{0.3}\text{Fe}_2\text{O}_4$ nanoparticles embedded in graphene oxide matrix, and studies of wide-band tunable microwave absorption. *ACS Appl Mater Interfaces* 13(39): 46967-46979. <https://doi.org/10.1021/acsami.1c10241>